Synthesis and Photocatalytic Properties of Au-ZnSe Hybrid Nanorods for H_2 Generation

1. Background

Hybrid nanocrystals which integrate multiple component into a single nanoparticle at nanoscale has attracted much research interest in recent years [1-6]. The combination of several material enables the hybrid nanocrystals with synergetic optical and chemical properties [2]. Hybrid semiconductor-metal nanostructures, especially platinum (Pt) or gold (Au) nanoparticles decorated semiconductor nanocrystals, such as Au-CdSe[7], Pt-CdSe[8] Au-CdS[9], CdS-Pt, CdSe/CdS-Pt[10], Au-Cu_3P[4], and Au-Cu_2O[11] gained much attention because of the special property of these hybrid nanocrystals, such as the located surface Plasmon resonance effect (LSPR) of noble metals and outstanding charge separation ability[12]. Nobel semiconductor-metal hybrid nanoparticles like Au-CdSe, Pt-CdS work as co-catalyst by providing the active sites for reaction with lower activation barrier than semiconductors. The lifetime of charge carriers is also extended because of the enhanced rate of electron-hole separation.[12]

Based on this the effective light induced electron-hole separation, noble metal-hybrid nanoparticles such as Au-Cu_3P[4], CdS-Pt, CdSe/CdS-Pt[10] or CdSe/CdS-Pt-Au bimetallic nanoparticles[13] are widely applied in photo catalysis reaction like H_2 generation by water splitting. Some research also reported CdS Nanocrystals with a dinuclear cobalt catalyst[14] or CdS (($Mo–Bi)S_x$/CdS)[15] can be used for the selective photocatalytic CO_2 reduction. In addition, the applications of hybrid semiconductor-metal nanoparticles in photodynamic therapy, antifouling, wound healing, and photoinitiators for 3D-printing recently are also reported which expanded the application field of the distinctive nanomaterial. [6]

Among all these applications, the conversion of renewable solar energy to hydrogen, has attracted massive attention because of the growing crisis of fuel energy. Up to now, metal decorated hybrid II-VI semiconductor photo catalysts are mostly based on CdSe or CdS semiconductor nanocrystals benefit from their mature synthetic control on morphology, metal location and size and visible light absorption of band gap.

Compared with Cd-based II-VI semiconductor, Zn-based II-VI semiconductor is non-toxic and environmental friendly materials which makes it more compatible for bio-applications and has great potential in efficient photocatalytic generation of reactive oxygen species (ROS) [16]. But the synthesis control of Zn-based II-VI semiconductor and their noble metal-hybrid nanoparticles is still a challenge[17]. From the point of application in photocatalysis for H_2 generation, Zn-based II-VI semiconductors with wide bandgap (bulk ZnSe: 2.82 eV; bulk ZnS 3.66 eV)[18] absorb ultraviolet (UV) light from the solar while Cd-based heterostructure nanocrystals absorb visible light. As an important portion of solar power (7%), the complementary absorption of full spectrum solar energy for photo catalysis is important for energy harvesting.[19-20]

Based on this idea, we developed a new regime of Cd-free semiconductor-metal hybrid nanocrystals: Au-ZnSe nanorods with controlled Au tips in this research. The optical properties, morphology, metal selective growth mechanism and the photocatalytic H2 generation function is studied in detail.

2. Results and Discussion

2.1 Synthesis and Characterization of Au-ZnSe Hybrid Nanorod

For semiconductor-metal hybrid nanocrystals, two-step growth approach is widely applied in which semiconductor with different components and shape are firstly synthesized followed by the later growth of metals.[8, 21-22] A reverse crystal-growth method of Au-CdSe flower, tetrapod, and core/shell semiconductor-metal hybrid nanoparticles is also reported in which pre-synthesized Au particles work as seeds[23]. Comparing the two methods, the growth site and size of noble metals on semiconductors are easier to control when employing semiconductor as seeds than that of employing noble metals as seeds. For example, most semiconductor grow as flower shape instead of one-dimensional nanorods or Au-CdSe core shell structure while using Au as seed to grow CdSe nanoparticles.

Herein, we used a two-step method to synthesize Au-ZnSe nanorods. Firstly, uniform ZnSe nanorods were synthesized by a heat-up method according to a previously reported method with some modification [24] (Experiment details can be found in Experimental Section in the Supporting Information), typically, zinc acetate and selenium powder were employed as precursor, oleylamine and 1-dodecanethiol were employed as ligand and solvent to

synthesize ZnSe nanorods at 240°C in a standard Schleck line. Compared with long ZnSe nanowires synthesized in oleylamine, the ZnSe nanorods synthesized in the mixture of oleylamine and 1-dodecanethiol are shorted and thicker, the UV-Vis of nanorods is 360nm which is red shifted than long nanowires with absorption at 345 nm[25]. To find out the composition and crystal structure of synthesized nanorods, powder XRD characterization was done (Supporting information Figure. S1), the XRD patterns identified the structure of wurtzite ZnSe rather than ZnSeS alloy structure, which means the 1-dodecanethiol just worked as solvent and ligand instead of S precursor. The uniform ZnSe nanorods grown at 260°C with average dimension of 24.8±7.7 nm in length and 2.1±0.3 nm in diameter (The length and diameter distribution is shown as supporting information Figure.S1) were used to further grow Au.

For metal growth, Banin's group reported the growth of Pt nanocrystals onto CdSe nanorods and nanonets in aqueous media, they concluded that the pH conditions of the growth solution determined the different morphologies[26], but the size of Pt dots is too big which may lead to the lower H_2 generation efficiency. Compared with noble metal growth in aqueous solution, the control of size and site of metals is much easier in nonpolar solution, such as chloroform and toluene with the help of amines as surfactant[21, 27-28].

Based on these research, we employed $AuCl_3$ as gold precursor and dodecylamine as surfactant and reductant for Au growth on ZnSe nanorods in toluene in our research[8]. Typically $AuCl_3$ was firstly dissolved with dodecylamine in toluene by sonication as Au stock solution, then a predetermined dosage of Au stock solution was injected into ZnSe nanorods dispersed in toluene under N_2 protection, a detailed experimental method is presented in supporting information. The dodecylamine works as the ligand to stabilize the nanorods and also works as reductant for $AuCl_3$ reduction[1-2].

Some research reported the mechanism of Au growth, such as light-induced growth[22] and thermal-induced growth[29] . For thermal mechanism, small gold domains tend to grow along the rod body at higher temperature while fewer gold particles are found to grow along the rod body. The laser irradiation helped the growth of big Au tips on one end of nanorods[29]. For size control of the gold tips can be also fulfilled by controlling the concentration of the starting materials in which Au tips starts to grow at one end due to the surfactant-controlled

growth of CdSe nanorods. The growth of Au along the body of nanorod or tetropod can be controlled by increasing the amount of Au added.[2]

In our research, we grow the Au tips under ambient light at room temperature, the different condition is the ratio between Au and ZnSe particles. Figure 1 presents the UV-vis absorbance spectra of Au-ZnSe hybrid nanorods with different ratio between Au precursor and ZnSe nanorods used for Au growth. When small amount of Au precursor was used (Figure 1: 1), the final solution is colourless, the same as its original ZnSe nanorods solution and an absorption peak at 368 nm can be found corresponding to the bandgap of ZnSe nanorods, with increased Au precursor used (Figure 1: 2~4), the exciton absorption peak of ZnSe nanorods are quenched due to the plasma resonance effect of gold as long as the final solution becoming brown which confirmed the successful growth of Au tips on ZnSe nanorods.
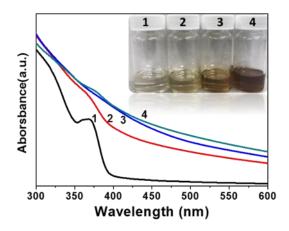

Figure 1. UV-vis absorbance spectra and of Au-ZnSe hybrid nanorods and a photo of solution after Au growth with different mass ratio between Au precursor and ZnSe nanorods; (1) m(AuCl$_3$: ZnSe nanorods) =1:10; (2) m(AuCl$_3$: ZnSe nanorods) =1:5; (3) m(AuCl$_3$: ZnSe nanorods) =3:5; (4) m(AuCl$_3$: ZnSe nanorods) =1:1;

Figure 2 shows TEM and STEM images of Au-ZnSe hybrid nanorods with different Au tip sizes and with narrow size distribution. As very small amount of Au precursor used for growth (m(AuCl$_3$: ZnSe nanorods) =1:10), almost no gold tip can be found grown on ZnSe nanorods (Supporting Information, Figure S2a), which interprets that the UV-Vis of this sample keeps almost the same as original ZnSe nanorods.

With more Au precursor used for growth, very small gold tips with a diameter 1.3 ± 0.2 nm are attached to ZnSe nanorods and most of gold tips are found to grow on one end. This phenomenon is similar to gold growth on CdSe nanorods reported by Mokari and Banin[3] in which one-sided growth is dominate at the first beginning and preceded by two-sided growth.

Further increase of mass ratio of $AuCl_3$ to ZnSe leads to the grow-up of small tips, in the meanwhile, gold tips with a diameter of 1.6 ± 0.3 nm are found grown on both ends of ZnSe nanorods. While the mass ratio of $AuCl_3$ to ZnSe gets to 1:1, bigger gold tips with a diameter of 2.2 ± 0.3 nm are found grown on both ends of ZnSe nanorods, some gold tips are also found to grown on the body of ZnSe nanorods. STEM-EDS mapping was done as a supplement to identify the growth of Au on ZnSe nanorods, Au tips were found to grow on the end of ZnSe nanorods in this research (Figure S3).

The site selection of gold growth can be also found in other regime, such as Au-CdSe[2] or Pt-CdS[21], the reason of site selection is the difference of binding energy (or reaction activity) of nanocrystal facets.

On the one hand, there is less ligand on the end of nanorods than its body, it's easier for gold precursor to contact with ZnSe nanorods. On the other hand, as we analysed before, the end facet of wurtzite ZnSe nanorods is (002), while the body surface of ZnSe nanorods is (100), the binding energy of these two facet is also different which leads to the selective growth of gold. The (002) planes are alternately composed of either Zn or Se atoms, which makes growth at earlier stages more favourable on the Se rich facets and leads to one-tip Au-ZnSe nanorods[21]. While more Au precursor was used for growth, the chemical potential of concentrated Au precursor overcame the energy barrier and grew to ZnSe nanorods.

What's more, when excessive Au precursor was used, big Au tips and aggregation phenomena can be found (Supporting Information, Figure S2b). The big Au tips can be found on the end of ZnSe nanorods which are caused by the ripening process[3] when high gold concentration was used.
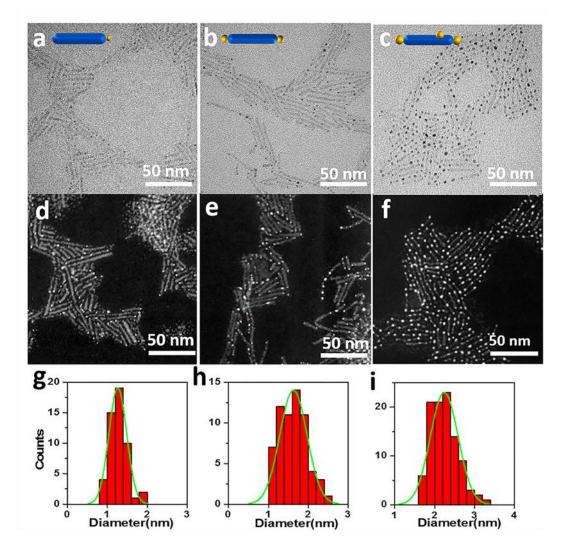
Figure 2. TEM images of Au-ZnSe hybrid nanorods with variable Au tip size of 1.3 ± 0.2 nm (a); 1.6 ± 0.3 nm (b); 2.2 ± 0.3 nm (c); (d-e) STEM images corresponding to (a-c); (g-i) size distribution histogram of the Au metal tip diameters corresponding to (a-c)

The detailed characterization of crystalline structure for Au-ZnSe hybrid nanorods is shown in Figure 3a. The X-ray diffraction (XRD) pattern of the Au-ZnSe hybrid nanorods shows that ZnSe nanorods are wurtzite structure (PDF Card #80-0008) and Au tips are cubic face-centred structure (PDF#99-0056). A high-resolution TEM (HRTEM) image and FFT patterns of a single Au nanocrystal is shown as Figure 3b. The lattice plane spacing of 0.235 and 0.204 nm agrees well with the (111) and (200) lattice planes of the Au crystal, respectively. It's worth noting that due to the big difference of mass between Au and Zn, Se atom, ZnSe nanorods are hard to see at high magnification while lattice of Au can be found clearly.
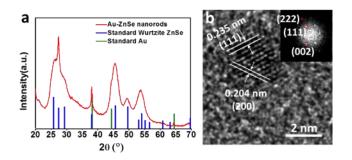
Figure 3. (a) XRD pattern (b) HRTEM images and FFT patterns of Au-ZnSe hybrid nanorods

In order to investigate the oxidation state of the Au domains present on the nanorods, we have studied X-ray photoelectron spectroscopy (XPS) of Au-ZnSe hybrid nanorods. The results of the XPS analysis are shown in Figure 4.

The XPS survey spectrum in Figure 4a of the clean Au-ZnSe hybrid nanorods powder confirmed the presence of Zn, Se, and Au signals.

The binding energy peaks at ≈84 eV and ≈87.7 eV of high resolution XPS spectra of Au are attributed to Au $4f_{7/2}$ and $4f_{5/2}$ in its zero oxidation state (Figure 4b)[30]. The distinct peaks observed at ≈84.9 eV and ≈88.6 eV are correspond to $4f_{7/2}$ and $4f_{5/2}$ binding energy peaks of Au in its plus one oxidation state[31]. This can be explained as most of the AuCl3 precursor is reduced to zero oxidation state while a small part of $AuCl_3$ is reduced to plus one oxidation state.

The two Zn 2p peaks at 1044.3 eV and 1021.3 eV in Figure 4b correspond to Zn $2p_{1/2}$ and $2p_{3/2}$ and confirm the presence of Zn^{2+} (Figure 4c)[32] . The corresponding binding energy values of Zn^{2+} can be attributed to Zn-Se bonding in ZnSe crystal.

The spectrum for Se (3d) was fitted yielding a single peak at the binding energy of 54.0 eV, which confirms the selenide phase in metal chalcogenides and is well in agreement with values reported for the Se^{2-} phase (Figure 4d) [32]. The Se 3d singlet peak is significantly broadened over a range of ~4 eV and it includes Se $3d_{5/2}$ and $3d_{3/2}$ due to an apparent lack of distinguishable peaks[32].

As analysed above, the values of binding energies for Zn and Se confirms the valance states as Zn^{2+} and Se^{2-} respectively. Most Au tips are of zero oxidation state and a small amount of Au precursor residue also exists as Au^+ in the final products.
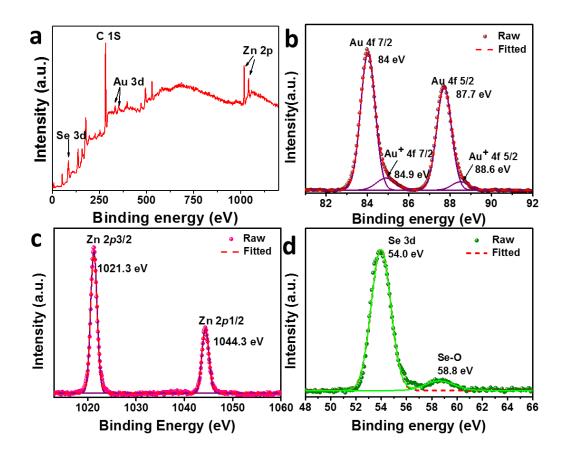

Figure 4. XPS spectra of the Au-ZnSe hybrid nanorods; (a) Survey spectrum of Au-ZnSe nanorods; (b) Binding energy peak of Au 4f; (c) Zn 2p; (d) Se 3d;

2.2 Simulation of Au-ZnSe Hybrid Nanorod growth

The growth direction of Au tips on ZnSe nanorods is measured by HRTEM. Based on the statics (Supporting Information, Figure S4) of the angel between (111) facet of Au tips and (100) facet of ZnSe nanorods, the angles are 0~90° without any angles of high frequency, so we concluded that gold was seldom growth on ZnSe nanorods without particular orientation. To further explore the atomic interfce structure between ZnSe nanorods and Au tips, simulations based on density functional theory (DFT) were performed.

DFT calculations were performed using the Vienna *Ab initio* Simulations Package (VASP) [33-34] and projected augmented wave (PAW) [35-37] method (with $1s^1$, $5d^{10}6s^1$, $4s^24p^4$, $3d^{10}4s^2$ as

valence electrons for H, Au, Se and Zn, respectively). The exchange-correlation interaction was treated with generalized gradient approximation (GGA) in the Perdew, Burke and Ernzerhof (PBE) [38] parameterization. The cutoff energy of plane-wave basis was set to 450 eV for ZnSe and 400 eV for Au. Integrations over the first Brillouin zone were calculated using a Gamma-centred **k**-point set of 6×6×4 for wurtzite ZnSe (space group *P6₃mc*, No. 186) and 12×2×12 for fcc Au. With these settings, the total energy was able to converge within 1 meV/atom. The structures were fully relaxed using PBE, and the energy was converged within 10^{-6} eV/cell and the force was converged to less than 10^{-4} eV/Å. We adopted GGA+U (U=8 and J=1) [39-40] to correct the self-interaction and over delocalized *d* states in wurtzite ZnSe.

Although the HRTEM measurements suggest no preference of a specific orientation relationship between ZnSe and Au, we think the interface between ZnSe (001) and Au (111) is a typical and representative structure of the hybrid system, as it is composed of the most closely packed planes and resembles the Au-CdSe hybrid system. The detailed interface structure of ZnSe (001) and Au (111) was explored thoroughly as follows: First, we scanned the potential energy surface (PES) of interfacing ZnSe (001) and Au (111). We built a 3x3x4 supercell of wurtzite ZnSe containing 16 alternating Zn and Se layers along (001), of which the top 11 layers were removed. The remained layers are terminated by Zn. We then removed the top Zn layer and added four fcc Au (111) layers on top. The Au fcc lattice is therefore subjected to a strain of 1.4%, which is within the DFT error. We then mapped the PES of this interface structure (denoted as ZnSe(001)//Au(111)) by moving around the Au layers together. The interfacing Se layer and four Au (111) layers were allowed to relax completely except that the in-plane coordinates of the top Au (111) layer and the other ZnSe layers were fixed. All the PES calculations for the interface were performed at the PBE level and with an energy cutoff of 450 eV and a single Gamma point sampling. The obtained PES is plotted in Figure 5. It can be seen that the highest barrier between energy minima is no more than 0.1 eV/atom, which implies no strong preference of specific interface structures. It can be inferred that when the first atomic layer of Au was deposited on the ZnSe (001) surface the distribution of Au atoms could be rather random since there is no big difference between different bonding states. The following build-up of Au layers will gain an orientation depending on the deposited Au layer, and thus an interface with no preference

of orientation relationship between ZnSe (001) and Au will be seen, which agrees with and explains the HRTEM observations.
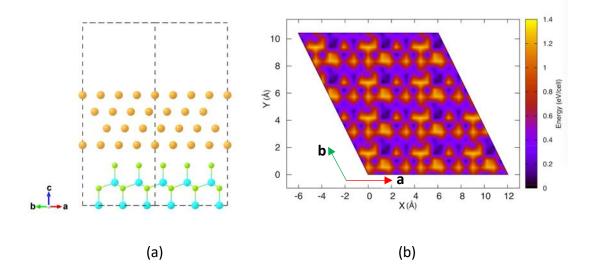

(a)　　　　　　　　　　　　　　　　　　(b)

Figure 5. (a) Initial input interface structure for potential energy surface calculations of ZnSe(001)/Au(111) interface; (b) Calculated potential energy surface of ZnSe(001)/Au(111) interface.

We then further explored the detailed atomic interface structure. The interface structure with the minimum energy was chosen and relaxed with a Monkhorst-Pack **k**-point set of $2 \times 2 \times 1$. Seven Au atoms at the interface layer that are most distant from ZnSe lattice sites were removed to create a ZnSe(001)/Zn_0Au_1/Au(111) interface, namely, an interface with the top layer Zn atoms completely substituted by the interfacing layer Au atoms and no more Au left in the interfacing Au single layer. From the ZnSe(001)/Zn_0Au_1/Au(111) interface, we varied the ratio of Zn to Au at the interfacing single layer to obtain the ZnSe(001)/$Zn_{1/3}Au_{2/3}$/Au(111), ZnSe(001)/$Zn_{2/3}Au_{1/3}$/Au(111) , and ZnSe(001)/Zn_1Au_0/Au(111) structures. The phase diagram of the interface can be obtained and is plotted in Figure 6. It can be seen that only the ZnSe(001)//Au(111) and ZnSe(001)/Zn_1Au_0/Au(111) interfaces are thermodynamically stable within the allowed chemical potentials of Zn and Au. The other three structures (ZnSe(001)/$Zn_{1/3}Au_{2/3}$/Au(111), ZnSe(001)/$Zn_{2/3}Au_{1/3}$/Au(111) , and ZnSe(001)/Zn_0Au_1/Au(111) structures) are not stable at all. Actuallly, the stable ZnSe(001)//Au(111) and ZnSe(001)/Zn_1Au_0/Au(111) interfaces representing the two situations: The interfacing of the Se-terminated nanorod end and the

Zn-terminated ZnSe nanorod end with Au (111), respectively. Therefore, at the high chemical potential of Au (low ratio of $AuCl_3$ to ZnSe), it could only allow the Se-terminated ZnSe nanorod end to grow Au tips, forming the ZnSe(001)//Au(111) interface. With the chemical potential of Au being lowered with more added $AuCl_3$, the ZnSe(001)/Zn_1Au_0/Au(111) interface is also allowed.
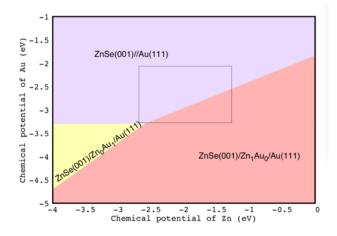

Figure 6. Phase diagram of ZnSe(001)/Au(111) interface. Five structures were explored, namely, the ZnSe(001)//Au(111), ZnSe(001)/Zn_0Au_1/Au(111), ZnSe(001)/$Zn_{1/3}Au_{2/3}$/Au(111), ZnSe(001)/$Zn_{2/3}Au_{1/3}$/Au(111) , and ZnSe(001)/Zn_1Au_0/Au(111). The ZnSe(001)/$Zn_{1/3}Au_{2/3}$/Au(111) and ZnSe(001)/$Zn_{2/3}Au_{1/3}$/Au(111) interfaces thermodynamically are not stable. The inset rectangular represents the allowed chemical potentials of Zn and Au. The chemical potential of Zn is bounded by $\mu_{ZnSe} - \mu_{Se} < \mu_{Zn} < \mu_{hcp-Zn}$, and the chemical potential of Au is bounded by $\mu_{fcc-Au} < \mu_{Au} < \mu_{AuSe} + \mu_{Zn} - \mu_{ZnSe}$.

2.3 Au-ZnSe Hybrid Nanorods for Photocatalytic H2 Generation

The hybrid Au-ZnSe may present novel catalytic property with hot electrons due to the plasma coupling effect of Au tips, compared with original ZnSe nanorods. The light induced electron-hole pair produced in ZnSe nanorods can gain a longer lifetime and a lower recombination rate as a result of the enhanced separation of charge carriers in the Au-ZnSe semiconductor-metal heterostructure.
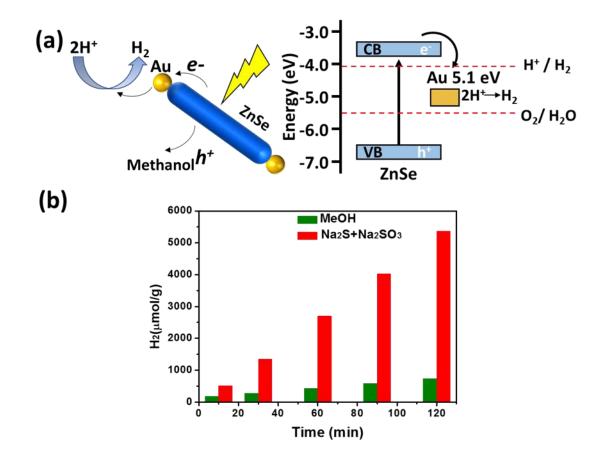
Figure 8. (a) Proposed photocatalytic mechanism of Au-ZnSe hybrid nanorods for H_2 production in water splitting and energy band alignment diagram; (b) Photocatalytic H_2 production of Au-ZnSe hybrid nanorods using methanol or Na_2S and Na_2SO_3 as sacrificial holes scavenger.

Figure 8a shows the band diagram of Au-ZnSe hybrid nanorods. The energy band gap of bulk ZnSe is 2.82 eV, light induced electrons are transferred to the conduction band of ZnSe followed by transferred to gold tips due to the band alignment between ZnSe[42-44] and Fermi level of Au[45] . The light induced holes keep in the valence band, thus the electron-hole are effectively separated and recombination is greatly reduced. Rich in electrons, the Au tips provide an active site for protons reduction and produce H_2 efficiently while the holes in ZnSe nanorods can be removed by introduction of methanol or Na_2S and Na_2SO_3.

 The photocatalytic activity of the hybrid nanoparticles was measured via the light-induced reduction of water using a 300W Xeon lamp (Newport, 200~2500 nm) to produce hydrogen

in the presence of methanol acting as sacrificial hole scavengers as depicted schematically in Figure 8.

The sample we used for photocatalyst is Au-ZnSe with two tips because according to previous report by Amirav[46] in which Pt-decorated CdSe@CdS rods with less reduction sites is more active for hydrogen reduction. As reported in Au-CdS NRs for photo catalysis, the size of metal tips has essential influence on reduction efficiency, Au-CdS NRs with a diameter of ~3 nm of Au tips showed the higher H_2 generation rate than Au-CdS NRs with a diameter of ~6 nm of Au tips [28]. Considering the combined influence of the metal tips number and size, we chose double-tips Au-ZnSe naorods with Au diameter of 1.6 ± 0.3 nm for photo catalysis characterization. PEI coating which make nanoparticles water soluble[47] and enhance the photocatalytic H_2 generation[48] was used for the colloidal synthesized Au-ZnSe nanoparticles[49].

As shown in Figure 8b, the photocatalytic H_2 production rate of Au-ZnSe hybrid nanorods with two gold tips is about 427 $\mu mol \cdot h^{-1} \cdot g^{-1}$ which is higher than reported H_2 evolution of Au@CdS (~100 $\mu mol \cdot h^{-1} \cdot g^{-1}$) CdS/Pt (~300 $\mu mol \cdot h^{-1} \cdot g^{-1}$) hybrid nanocrystals and the generation kinetics shows that the H_2 generation is stable and sustainable[50].

In previous reports of photocatalytic hydrogen evolution reaction (HER) with noble metal decorated II-VI nanocrystals as catalyst, the removal of holes from the surface of the nanocrystals to the electron donor has been illustrated as the key rate limiting and Na_2S and Na_2SO_3 can remove holes more efficiently than methanol[10]. So we conducted another test with applying Na_2S and Na_2SO_3 as sacrificial holes scavenger, the photocatalytic H2 production rate is 2696 $\mu mol \cdot h^{-1} \cdot g^{-1}$ which is much higher than that of using methanol as sacrificial holes scavenger.

We also investigate the HER by using the free energy of hydrogen adsorption (ΔG_{H*}, * denotes the electrode) as a single catalytic descriptor [41]. This descriptor can decribe the hydrogen evolution exchange-current density

$$i_0 = -ek_0 \frac{1}{1 + \exp(-\Delta G_{H*}/kT)}$$

Where i_0 is the hydrogen evolution exchange-current density, e is the electron charge, and k_0 is a factor that needs to be fitted to experimental data. The best electrode material should have ($\Delta G_{H*} = 0$) for hydrogen evolution reaction
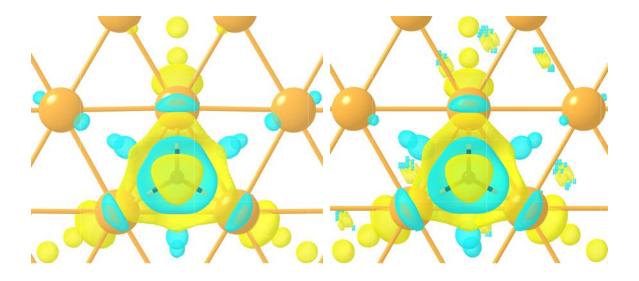
$$H^+ + e^- + * \rightarrow \frac{1}{2} H_2(g)$$

ΔG_{H*}, therefore, can be expressed by

$$\Delta G_{H*} = \Delta E_H + \Delta E_{ZPE} - T\Delta S_H$$

where ΔE_H, ΔE_{ZPE}, and ΔS_H are the potential energy difference, zero-point energy difference and change of entropy, respectively. At 300 K, it can be simplified as $\Delta G_{H*} = \Delta E_H + 0.24\ eV$ [41].

The calculated HER free energies were summarized in Table 1. All the stable interfaces show much smaller $|\Delta G_{H*}|$ compared to the pristine Au (111) surface. This is due to the enhanced adsorption of H* by the Au atoms of interface structures. At a close look, the interface structures show an increased charge redistribution upon hydrogen adsorption as can be seen from the differential charge density plot in Figure 7. Hydrogen adsorbed on the hybrid Zn-AuSe (Figure 7b) gains more charge than the hydrogen on pristine Au (Figure 7a).

Figure 7. Differential charge density plot for hydrogen adsorption onto a fcc site of (a) pristine Au (111) and (b) top Au (111) of ZnSe(001)//Au(111) interface. Golden and black balls indicate the Au and H atoms, respectively. Yellow and cyan indicate the charge loss and gain, respectively. Isosurface value is 0.001 e/Å^3.

Table 1. Calculated free energy change for hydrogen evolution on different electrodes.

Electrode	$\lvert\Delta G_{H*}\rvert$ (eV)	
	fcc site	*hcp* site
Au (111)	0.38	0.43
ZnSe(001)//Au(111)	0.28	0.27
ZnSe(001)/Zn$_1$Au$_0$/Au(111)	0.15	0.24
ZnSe(001)/Zn$_0$Au$_1$/Au(111)	0.10	0.26

3. Conclusion

We have successfully synthesized novel Cd-free Au-ZnSe semiconductor-metal nanorods by growing Au tips of variable diameter and site on ZnSe NRs. Au tips are found to preferably grow on one end of ZnSe NRs then to two ends, followed by the body depending on the concentration of used Au precursor. Au tips tend to be aggregated if large amount of gold precursor is used for growth. The novel Cd-free system we developed showed the plasma coupling effect of gold and high H_2 generation rate as photo catalyst for water splitting. The photocatalytic H_2 production rate is 427 μmol·h^{-1}·g^{-1} and 2696 μmol·h^{-1}·g^{-1} while employing methanol or Na_2S and Na_2SO_3 as sacrificial holes scavenger respectively. This performance is comparable with Cd-based semiconductor-metal heterostructure nanocrystals and could even be further improved, focusing on the variation of noble metal species, such as Pt or

alloyed Au-Pt or combined metals, as well as the variation of size and number of noble metal domains present on the NRs. This system open a new Cd-free system plat for H_2 generation by water splitting and the special structure can be also used for redox reaction on biochemistry owing to its non-toxicity.

Reference.

1.   Mokari, T.; Banin, U., Synthesis and Properties of CdSe/ZnS Core/Shell Nanorods. *Chem. Mater.* **2003,** *15* (20), 3955-3960.

2.   Mokari, T.; Rothenberg, E.; Popov, I.; Costi, R.; Banin, U., Selective growth of metal tips onto semiconductor quantum rods and tetrapods. *Science* **2004,** *304* (5678), 1787-90.

3.   Mokari, T.; Sztrum, C. G.; Salant, A.; Rabani, E.; Banin, U., Formation of asymmetric one-sided metal-tipped semiconductor nanocrystal dots and rods. *Nat. Mater.* **2005,** *4* (11), 855-863.

4.   Dutta, A.; Dutta, S. K.; Mehetor, S. K.; Mondal, I.; Pal, U.; Pradhan, N., Oriented Attachments and Formation of Ring-on-Disk Heterostructure Au–Cu3P Photocatalysts. *Chem. Mater.* **2016,** *28* (6), 1872-1878.

5.   Costi, R.; Saunders, A. E.; Banin, U., Colloidal hybrid nanostructures: a new type of functional materials. *Angew. Chem. Int. Ed.* **2010,** *49* (29), 4878-97.

6.   Waiskopf, N.; Ben-Shahar, Y.; Banin, U., Photocatalytic Hybrid Semiconductor-Metal Nanoparticles; from Synergistic Properties to Emerging Applications. *Adv. Mater.* **2018,** *30* (41), e1706697.

7.   Figuerola, A.; van Huis, M.; Zanella, M.; Genovese, A.; Marras, S.; Falqui, A.; Zandbergen, H. W.; Cingolani, R.; Manna, L., Epitaxial CdSe-Au nanocrystal heterostructures by thermal annealing. *Nano Lett.* **2010,** *10* (8), 3028-36.

8.   Naskar, S.; Schlosser, A.; Miethe, J. F.; Steinbach, F.; Feldhoff, A.; Bigall, N. C., Site-Selective Noble Metal Growth on CdSe Nanoplatelets. *Chem. Mater.* **2015,** *27* (8), 3159-3166.

9.   Van Huis, M. A.; Figuerola, A.; Fang, C.; Beche, A.; Zandbergen, H. W.; Manna, L., Chemical transformation of Au-tipped CdS nanorods into AuS/Cd core/shell particles by electron beam irradiation. *Nano Lett.* **2011,** *11* (11), 4555-61.

10.   Wu, K.; Chen, Z.; Lv, H.; Zhu, H.; Hill, C. L.; Lian, T., Hole removal rate limits photodriven H2 generation efficiency in CdS-Pt and CdSe/CdS-Pt semiconductor nanorod-metal tip heterostructures. *J. Am. Chem. Soc.* **2014,** *136* (21), 7708-16.

11.   Asenath-Smith, E.; Noble, J. M.; Hovden, R.; Uhl, A. M.; DiCorato, A.; Kim, Y.-Y.; Kulak, A. N.; Meldrum, F. C.; Kourkoutis, L. F.; Estroff, L. A., Physical Confinement Promoting Formation of Cu2O–

Au Heterostructures with Au Nanoparticles Entrapped within Crystalline Cu2O Nanorods. *Chem. Mater.* **2016,** *29* (2), 555-563.

12.   Linic, S.; Christopher, P.; Ingram, D. B., Plasmonic-metal nanostructures for efficient conversion of solar to chemical energy. *Nat. Mater.* **2011,** *10* (12), 911-21.

13.   Kalisman, P.; Houben, L.; Aronovitch, E.; Kauffmann, Y.; Bar-Sadan, M.; Amirav, L., The golden gate to photocatalytic hydrogen production. *J. Phys. Chem. A* **2015,** *3* (39), 19679-19682.

14.   Bi, Q. Q.; Wang, J. W.; Lv, J. X.; Wang, J.; Zhang, W.; Lu, T. B., Selective Photocatalytic CO2 Reduction in Water by Electrostatic Assembly of CdS Nanocrystals with a Dinuclear Cobalt Catalyst. *ACS Catal.* **2018,** *8* (12), 11815-11821.

15.   Zhou, B.; Song, J.; Xie, C.; Chen, C.; Qian, Q.; Han, B., Mo–Bi–Cd Ternary Metal Chalcogenides: Highly Efficient Photocatalyst for CO2 Reduction to Formic Acid Under Visible Light. *ACS Sustainable Chem. Eng* **2018,** *6* (5), 5754-5759.

16.   Waiskopf, N.; Ben-Shahar, Y.; Galchenko, M.; Carmel, I.; Moshitzky, G.; Soreq, H.; Banin, U., Photocatalytic Reactive Oxygen Species Formation by Semiconductor-Metal Hybrid Nanoparticles. Toward Light-Induced Modulation of Biological Processes. *Nano Lett.* **2016,** *16* (7), 4266-73.

17.   Bose, R.; Wasey, A. H.; Das, G. P.; Pradhan, N., Heteroepitaxial Junction in Au-ZnSe Nanostructure: Experiment versus First-Principle Simulation. *J. Phys. Chem. Lett.* **2014,** *5* (11), 1892-8.

18.   Bechiri, A.; Benmakhlouf, F.; Bouarissa, N., Calculation of electronic and optical properties of Zn-based II–VI semiconductors. *Phys. Procedia.* **2009,** *2* (3), 803-812.

19.   Wu, Z.; Wang, W.; Cao, Y.; He, J.; Luo, Q.; Bhutto, W. A.; Li, S.; Kang, J., A beyond near-infrared response in a wide-bandgap ZnO/ZnSe coaxial nanowire solar cell by pseudomorphic layers. *J. Mater. Chem. A* **2014,** *2* (35), 14571.

20.   Zhuang, T.-T.; Liu, Y.; Li, Y.; Zhao, Y.; Wu, L.; Jiang, J.; Yu, S.-H., Integration of Semiconducting Sulfides for Full-Spectrum Solar Energy Absorption and Efficient Charge Separation. *Angew. Chem., Int. Ed..* **2016,** *55* (22), 6396-6400.

21.   Habas, S. E.; Yang, P.; Mokari, T., Selective Growth of Metal and Binary Metal Tips on CdS Nanorods. *J. Am. Chem. Soc.* **2008,** *130* (11), 3294-3295.

22.   Carbone, L.; Jakab, A.; Khalavka, Y.; Sonnichsen, C., Light-Controlled One-Sided Growth of Large Plasmonic Gold Domains on Quantum Rods Observed on the Single Particle Level. *Nano Lett.* **2009,** *9* (11), 3710-4.

23.   Haldar, K. K.; Pradhan, N.; Patra, A., Formation of heteroepitaxy in different shapes of Au-CdSe metal-semiconductor hybrid nanostructures. *Small* **2013,** *9* (20), 3424-32.

24.   Selvaraj, J.; Mahesh, A.; Asokan, V.; Baskaralingam, V.; Dhayalan, A.; Paramasivam, T., Phosphine-Free, Highly Emissive, Water-Soluble Mn:ZnSe/ZnS Core–Shell Nanorods: Synthesis, Characterization, and in Vitro Bioimaging of HEK293 and HeLa Cells. *ACS Appl. Nano Mater.* **2017,** *1* (1), 371-383.

25.   Jia, G.; Banin, U., A general strategy for synthesizing colloidal semiconductor zinc chalcogenide quantum rods. *J. Am. Chem. Soc.* **2014,** *136* (31), 11121-7.

26.   Elmalem, E.; Saunders, A. E.; Costi, R.; Salant, A.; Banin, U., Growth of Photocatalytic CdSe-Pt Nanorods and Nanonets. *Adv. Mater.* **2008,** *20* (22), 4312-4317.

27.   Costi, R.; Saunders, A. E.; Elmalem, E.; Salant, A.; Banin, U., Visible Light-Induced Charge Retention and Photocatalysis with Hybrid CdSe–Au Nanodumbbells. *Nano Lett.* **2008,** *8* (2), 637-641.

28.   Ben-Shahar, Y.; Scotognella, F.; Kriegel, I.; Moretti, L.; Cerullo, G.; Rabani, E.; Banin, U., Optimal metal domain size for photocatalysis with hybrid semiconductor-metal nanorods. *Nat. Commun.* **2016,** *7*, 10413.

29.   Menagen, G.; Macdonald, J. E.; Shemesh, Y.; Popov, I.; Banin, U., Au Growth on Semiconductor Nanorods: Photoinduced versus Thermal Growth Mechanisms. *J. Am. Chem. Soc.* **2009,** *131* (47), 17406-17411.

30.   Kwon, K. C.; Kim, B. J.; Lee, J.-L.; Kim, S. Y., Effect of anions in Au complexes on doping and degradation of graphene. *J. Mater. Chem. C* **2013,** *1* (13), 2463.

31.   Villa, A.; Dimitratos, N.; Chan-Thaw, C. E.; Hammond, C.; Veith, G. M.; Wang, D.; Manzoli, M.; Prati, L.; Hutchings, G. J., Characterisation of gold catalysts. *Chem. Soc. Rev.* **2016,** *45* (18), 4953-94.

32.   Bagade, C. S.; Mali, S. S.; Ghanwat, V. B.; Khot, K. V.; Patil, P. B.; Kharade, S. D.; Mane, R. M.; Desai, N. D.; Hong, C. K.; Patil, P. S.; Bhosale, P. N., A facile and low cost strategy to synthesize Cd1−xZnxSe thin films for photoelectrochemical performance: effect of zinc content. *RSC Adv.* **2015,** *5* (69), 55658-55668.

33.   Kresse, G.; Joubert, D., From ultrasoft pseudopotentials to the projector augmented-wave method. *Phys. Rev. B* **1999,** *59* (3), 1758.

34.   Blöchl, P. E., Projector augmented-wave method. *Phys. Rev. B* **1994,** *50* (24), 17953.

35.   Kresse, G.; Furthmüller, J., Efficiency of *ab-initio* total energy calculations for metals and semiconductors using a plane-wave basis set. *Comput. Mater. Sci.* **1996,** *6* (1), 15--50.

36.   Kresse, G.; Furthmüller, J., Efficient iterative schemes for *ab initio* total-energy calculations using a plane-wave basis set. *Phys. Rev. B* **1996,** *54* (16), 11169.

37.   Kresse, G.; Hafner, J., *Ab initio* molecular dynamics for open-shell transition metals. *Phys. Rev. B* **1993,** *48* (17), 13115.

38.   Perdew, J. P.; Burke, K.; Ernzerhof, M., Generalized gradient approximation made simple. *Phys. Rev. Lett.* **1996,** *77* (18), 3865--3868.

39.   Dudarev, S. L.; Botton, G. A.; Savrasov, S. Y.; Humphreys, C. J.; Sutton, A. P., Electron-energy-loss spectra and the structural stability of nickel oxide: An LSDA+U study. *Phys. Rev. B* **1998,** *57* (3), 1505-1509.

40.   Miyake, T.; Zhang, P.; Cohen, M. L.; Louie, S. G., Quasiparticle energy of semicore *d* electrons in ZnS: Combined LDA+U and GW approach. *Phys. Rev. B* **2006,** *74* (24), 245213.

41.   Nørskov, J. K.; Bligaard, T.; Logadottir, A.; Kitchin, J. R.; Chen, J. G.; Pandelov, S.; Stimming, U., Trends in the Exchange Current for Hydrogen Evolution. *J. Electrochem. Soc.* **2005,** *152* (3), J23-J26.

42.   Oh, N.; Nam, S.; Zhai, Y.; Deshpande, K.; Trefonas, P.; Shim, M., Double-heterojunction nanorods. *Nat. Commun.* **2014,** *5*, 3642.

43.   Wang, A.; Shen, H.; Zang, S.; Lin, Q.; Wang, H.; Qian, L.; Niu, J.; Song Li, L., Bright, efficient, and color-stable violet ZnSe-based quantum dot light-emitting diodes. *Nanoscale* **2015,** *7* (7), 2951-9.

44.   Zhou, J.; Zhuang, H. L.; Wang, H., Layered tetragonal zinc chalcogenides for energy-related applications: from photocatalysts for water splitting to cathode materials for Li-ion batteries. *Nanoscale* **2017,** *9* (44), 17303-17311.

45.   Xiang, X.; Chou, L.; Li, X., Synthesis of PdS-CdSe@CdS-Au nanorods with asymmetric tips with improved H 2 production efficiency in water splitting and increased photostability. *Chin. J. Cata* **2018,** *39* (3), 407-412.

46.   Nakibli, Y.; Kalisman, P.; Amirav, L., Less Is More: The Case of Metal Cocatalysts. *J. Phys. Chem. Lett.* **2015,** *6* (12), 2265-8.

47.   Pang, F.; Zhang, R.; Lan, D.; Ge, J., Synthesis of Magnetite-Semiconductor-Metal Trimer Nanoparticles through Functional Modular Assembly: A Magnetically Separable Photocatalyst with Photothermic Enhancement for Water Reduction. *ACS Appl. Mater. Interfaces* **2018,** *10* (5), 4929-4936.

48.   Wen, M.; Li, X. B.; Jian, J. X.; Wang, X. Z.; Wu, H. L.; Chen, B.; Tung, C. H.; Wu, L. Z., Secondary coordination sphere accelerates hole transfer for enhanced hydrogen photogeneration from [FeFe]-hydrogenase mimic and CdSe QDs in water. *Sci. Rep.* **2016,** *6*, 29851.

49.   Ben-Shahar, Y.; Scotognella, F.; Waiskopf, N.; Kriegel, I.; Dal Conte, S.; Cerullo, G.; Banin, U., Effect of surface coating on the photocatalytic function of hybrid CdS-Au nanorods. *Small* **2015,** *11* (4), 462-71.

50.   Ma, L.; Chen, K.; Nan, F.; Wang, J.-H.; Yang, D.-J.; Zhou, L.; Wang, Q.-Q., Improved Hydrogen Production of Au-Pt-CdS Hetero-Nanostructures by Efficient Plasmon-Induced Multipathway Electron Transfer. *Adv. Funct. Mater.* **2016,** *26* (33), 6076-6083.